Title	Ab initio study of spin-spiral noncollinear magnetism in a free-standing Fe(110) monolayer under in-plane strain
Author(s)	Shimada, Takahiro; Okuno, Junichi; Kitamura, Takayuki
Citation	Physical Review B (2012), 85(13)
Issue Date	2012-04
URL	http://hdl.handle.net/2433/155716
Right	©2012 American Physical Society.
Type	Journal Article
Textversion	publisher

Ab initio study of spin-spiral noncollinear magnetism in a free-standing Fe(110) monolayer under in-plane strain

Takahiro Shimada,* Junichi Okuno, and Takayuki Kitamura
Department of Mechanical Engineering and Science, Kyoto University, Sakyo-ku, Kyoto 606-8501, Japan
(Received 27 February 2012; revised manuscript received 13 April 2012; published 24 April 2012)

We investigate the magnetic phase transition from collinear ferromagnetic (FM) ordering to noncollinear spin-spiral (SS) ordering in an Fe(110) monolayer under in-plane strain by performing fully unconstrained first-principles spin-density-functional calculations. The FM Fe(110) monolayer undergoes a FM-SS phase transition on the application of in-plane compression, whereas the application of tension keeps the system FM. The stability and wavelength of the excited SS state are further increased by compressive strains, especially along [$\bar{1}$10]. The FM-SS transition in the isotropically strained monolayer is dominated by competing exchange interactions between the ferromagnetically coupled first neighbor and the antiferromagnetically coupled second neighbor; the third neighbor also contributes to the transition under anisotropic strain. In addition, we demonstrate the stabilization mechanism of SS noncollinear magnetism from the electronic band structures: The noncollinear SS state is stabilized by a remarkable interband repulsion between the majority and minority spins, which occurs under in-plane compression.

DOI: 10.1103/PhysRevB.85.134440 PACS number(s): 75.75.−c, 73.22.−f, 31.15.A−

I. INTRODUCTION

In recent years, nanostructured magnetic materials, such as ultrathin films, nanowires, and nanodots, have attracted considerable attention because of their unique magnetic properties, which differ considerably from those of their respective bulk materials.[1–7] These nanoscale magnetic materials are promising for technological applications such as ultrahigh-density magnetic storage devices, magnetic sensors, and nanomotors.[8–11] Both scientific interest in the unusual magnetic properties of nanoscale components and the increasing demand to miniaturize magnetic devices drive researchers to synthesize and investigate magnetic nanostructures.

Recent advances have enabled extremely thin films of a few atomic layers to be fabricated.[12–16] In particular, an Fe monolayer that consists of a single (110) atomic layer of a body-centered-cubic lattice was fabricated by pseudomorphic growth on a W(110) substrate.[15] It has been intensively investigated both experimentally and theoretically.[5,15–24] Several studies have revealed that reduced dimensionality and symmetry breaking give rise to the exotic magnetic properties of the Fe(110) monolayer, such as an extremely narrow domain wall (DW) with a thickness of only 0.6 ± 0.2 nm,[15] and excitation of a noncollinear spin-spiral (SS) wave.[20–24]

The SS structure, whose magnetization vector continuously rotates in a certain direction in a crystal, is of great importance and interest to both fundamental and applied physics as a representative of noncollinear magnetism that occurs in nanostructures. However, the detailed excitation mechanism of the noncollinear SS state in the Fe(110) monolayer has not been elucidated yet. In addition, previous theoretical studies employed the local spin density approximation (LSDA) in density-functional theory (DFT), which failed to describe the ferromagnetic (FM) ground state of body-centered-cubic (bcc) iron.[25,26] Thus, using the LSDA functional can result in an incorrect prediction of the magnetic ground state of the Fe(110) monolayer, as discussed in Ref. 5. On the other hand, epitaxial strain introduced by a lattice mismatch between a film and a substrate often plays an important role in determining the magnetic ground state; for example, a FM-to-antiferromagnetic (AFM) phase transition has been observed in Fe(001) thin films.[4,27–32] Hence, the emergence of a noncollinear SS structure in the monolayer should be discussed by considering the effect of epitaxial in-plane strain.

Theoretical calculations based on DFT[33,34] within the generalized gradient approximation (GGA) have provided comprehensive insight into both collinear and noncollinear magnetism in nanostructures.[2,3,5,35–37] In the present study, we perform *ab initio* spin-density-functional calculations within the GGA to investigate the magnetic ground state and the noncollinear magnetism of the SS structure in an Fe(110) monolayer under various in-plane strains. Section II describes the methodologies used including the simulation models and procedure. Section III A describes the magnetic phase transition including the noncollinear SS structure in an Fe(110) monolayer under in-plane strain. In Sec. III B, the magnetic phase transition is discussed in terms of an exchange interaction by introducing an exchange parameter J. In Sec. III C, we demonstrate the stabilization mechanism of the SS structure based on electronic band structure analysis. Finally, Sec. IV summarizes the results.

II. COMPUTATIONAL DETAILS

A. Simulation method

Ab initio spin-density functional calculations are conducted using the Vienna Ab-initio Simulation Package (VASP) code.[38,39] The electronic wave functions are expanded in plane waves up to a cutoff kinetic energy of 500 eV. The electron-ion interaction is described by projector-augmented wave (PAW) potentials[40,41] that explicitly include the Fe 3*d* and 4*s* electrons in the valence states. Because the PAW approach has the computational efficiency of the pseudopotential method and the accuracy of the all-electron scheme, which avoids problems with linearizing the core-valence exchange interaction, PAW potentials can accurately describe magnetism in transition metal nanostructures.[42] The GGA proposed by

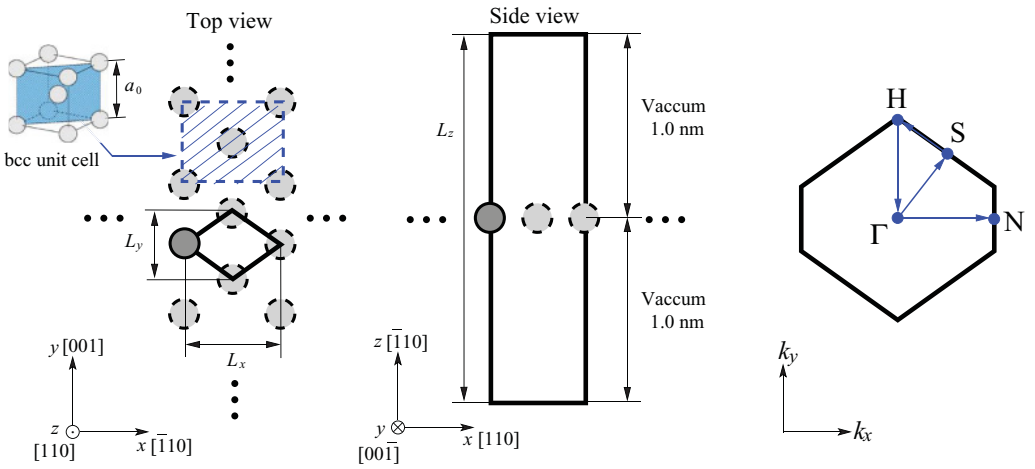

(a) Simulation model of Fe(110) monolayer (b) Brillouin zone

FIG. 1. (Color online) (a) Simulation model of an Fe(110) monolayer. The solid black box indicates the simulation cell. (b) First Brillouin zone of an Fe(110) monolayer.

Perdew, Burke, and Ernzerhof (PBE)[43] is used to evaluate the exchange-correlation energy because the GGA functional can accurately reproduce the structural and magnetic ground state of bcc iron.[4,5,27,44] A full vector-field description of the magnetization density that allows continuous variation in the direction of the local magnetic moments between atoms is required to accurately identify the noncollinear SS state. To this end, we perform fully unconstrained noncollinear magnetic calculations within the PAW formalism, as implemented in the VASP code by Hobbs *et al.*[45] In addition, we apply the generalized Bloch equations to analyze the incommensurate SS state.[46,47] The spin-orbit coupling (SOC) is explicitly included in the present calculations. The convergence criterion for self-consistent total-energy calculations is taken to be 1.0×10^{-6} eV/atom as the SS excitation energy and the magnetic configuration do not change further if a stricter convergence criterion is applied.

B. Simulation model and procedure

Figure 1(a) shows the simulation model of an Fe(110) monolayer, in which the in-plane x and y axes are $[\bar{1}10]$ and $[00\bar{1}]$, respectively. Since a three-dimensional periodic boundary condition is applied, a vacuum thickness of $l_v = 2.0$ nm is introduced in the z direction (perpendicular to the monolayer) to prevent undesirable interactions from neighboring monolayers. Thus, the simulation cell dimensions in the x, y, and z directions are initially set to $L_x = \sqrt{2}a$, $L_y = a$, and $L_z = 2.0$ nm, respectively, where a is the lattice constant of bulk bcc iron ($a = 0.287$ nm).[48] Brillouin-zone (BZ) integrations are performed with a $18 \times 18 \times 1$ Monkhorst-Pack k-point mesh.[49]

To systematically investigate the effect of in-plane strain, small strain increments, $\Delta\varepsilon_{xx}$ and $\Delta\varepsilon_{yy}$, are applied to the monolayer step by step. Here, we consider both isotropic ($\varepsilon_{xx} = \varepsilon_{yy}$) and anisotropic ($\varepsilon_{xx} \neq \varepsilon_{yy}$) strains. Noncollinear SS calculations are performed at each strain by varying the SS wave vector $\mathbf{q}$ within the first Brillouin zone, as illustrated in Fig. 1(b).

III. RESULTS AND DISCUSSION

A. Magnetic phase transition under in-plane strain

Figure 2 shows the SS excitation energy, $\Delta E = E_{\rm SS} - E_{\rm FM}$, as a function of the SS wave vector $\mathbf{q}$ along the Γ-S-H-Γ-N path in the Brillouin zone (i.e., the magnon dispersion relation) under various isotropic in-plane strain conditions, $\varepsilon_{xx} = \varepsilon_{yy}$. The SS structure with the wave vector $\mathbf{q} = (0,0)$ (Γ point) corresponds to the collinear FM state, while that with $\mathbf{q} = (2\pi/L_x, 0)$ (N point) corresponds to the collinear AFM state. Under the strain-free condition and tensile strains ($\varepsilon_{xx} = \varepsilon_{yy} \geqslant 0.0$), the minimum-energy point, $E_{\rm min}$, along the q path is located at Γ (i.e., the FM state is stable). On the other hand, negative SS excitation energies are found along the Γ-S, Γ-H, and Γ-N lines under compression ($\varepsilon_{xx} = \varepsilon_{yy} < 0.0$). The minimum energy structure is located along the Γ-N line [$\mathbf{q} = \frac{2\pi}{L_x}(q_x, 0)$], which indicates that the noncollinear SS state becomes energetically favorable with the wave vector along the

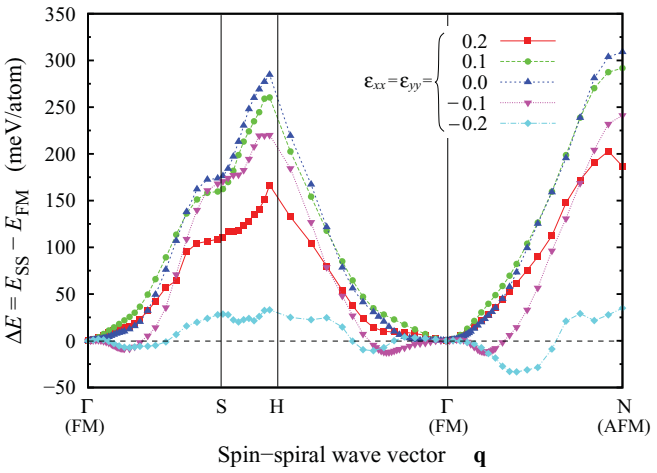

FIG. 2. (Color online) SS excitation energy, $\Delta E = E_{\rm SS} - E_{\rm FM}$, as a function of SS wave vector $\mathbf{q}$, along the Γ-S-H-Γ-N path in the Brillouin zone. Under various isotropic in-plane strains, $\varepsilon_{xx} = \varepsilon_{yy}$.

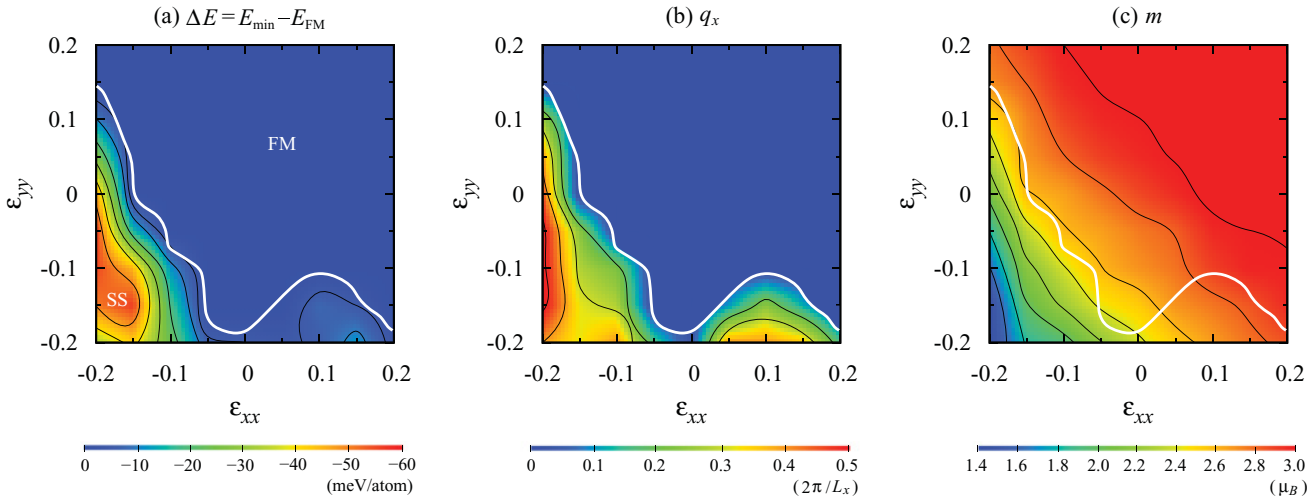

FIG. 3. (Color online) (a) SS wave excitation energy, $\Delta E = E_{\min} - E_{\mathrm{FM}}$, (b) SS wave vector q_x, and (c) magnitude of magnetic moment of Fe atom m, as functions of in-plane strains (ε_{xx}, ε_{yy}). The white lines indicate the FM-SS magnetic phase transition. For ΔE, the minimum energy in the Brillouin zone is taken at each strain.

x direction ([$\bar{1}$10]). Thus, the compressive strain involves the FM-SS magnetic phase transition in the Fe(110) monolayer.

Figure 3(a) plots the SS excitation energy, $\Delta E = E_{\min} - E_{\mathrm{FM}}$, for both isotropic and anisotropic strains. Here, the minimum SS excitation energy within $\mathbf{q}$ in the Brillouin zone is denoted by $E_{\min}$. Thus, the negative ΔE indicates the existence of a stable noncollinear SS ground state and the white line represents the FM-SS phase transition. The SS state also appears under anisotropic compression at approximately $\varepsilon_{xx} < -0.10$ or $\varepsilon_{yy} < -0.10$. However, the effects of ε_{xx} and ε_{yy} are not equivalent: ΔE under $\varepsilon_{xx} < -0.10$ is lower than that under $\varepsilon_{yy} < -0.10$. This indicates that the compression along [$\bar{1}$10] (the x direction) contributes more to the stability of the noncollinear SS state. [$\bar{1}$10] corresponds to the direction of the excited SS wave, as described below.

Note that the Fe monolayer pseudomorphically grown on a W(110) substrate[15,16] corresponds to the strain of (ε_{xx}, ε_{yy}) = (0.10,0.10) [the strain with respect to the equilibrium lattice parameters of the free-standing Fe monolayer, $L_x = 2.949$ Å and $L_y = 2.408$ Å, is (ε_{xx}, ε_{yy}) = (0.07,0.31)], where the magnetic ground state is FM. This is consistent with the FM ground state experimentally observed in the Fe monolayer on the W substrate.[15,16]

Figure 3(b) shows the SS wave vector $\mathbf{q}$ as functions of in-plane strains (ε_{xx}, ε_{yy}). In the present strain region, as the minimum SS excitation energy is always located along the Γ-N line in the Brillouin zone [$\mathbf{q} = \frac{2\pi}{L_x}(q_x,0)$], we show that the q_x value in the plot tends to increase smoothly as compressive strain is applied. A larger q_x(=0.4 ∼ 0.5) is found around $\varepsilon_{xx} = -0.20$, whereas q_x is smaller (0.1 ∼ 0.25) under $\varepsilon_{yy} = -0.20$. Thus, the compressive ε_{xx} affects the SS wave vector q_x more than ε_{yy}. This trend is similar to the strain dependence of ΔE [see the contour maps in Figs. 3(a) and 3(b)].

Figure 3(c) shows the magnitude of the magnetic moment m as a function of the in-plane strains. The magnetic moment increases smoothly with increasing tensile strain, whereas it decreases under compression. A similar trend was observed for thicker Fe(001) films.[4] However, the magnetic moment in the Fe monolayer seems to vary smoothly, even across the FM-SS transition line, whereas a discontinuous change in the magnetic moment was observed in thicker Fe(001) films that undergo a FM-AFM phase transition under in-plane compression.[4] This characteristic corresponds to the fact that the magnitude of m in the monolayer is less sensitive to the SS wave vector $\mathbf{q}$.

Note that the spin-orbit coupling does not appreciably affect both the FM-SS phase transition and the magnetic properties. This is because the magnetocrystalline anisotropy (MCA) energy of the free-standing Fe monolayer is smaller by two orders of magnitude than the exchange energy.[5]

Previous theoretical studies of Fe(110) monolayers have been performed within the LSDA on the exchange-correlation energy.[17–24] These studies found that the noncollinear SS state was the ground state of the Fe(110) monolayer under strain-free conditions,[20–24] but this clearly conflicts with the experimental observation that the monolayer remains in the FM ground state.[13,15] In addition, the LSDA functional gives a negative domain wall (DW) energy in the monolayer, $E_{\mathrm{DW}}^{\mathrm{ML}} = -6.5$ meV/atomic row[18], whereas the GGA functional provides a reasonable positive DW energy.[5] This probably originates from a well-known problem of the LSDA functional, namely its failure to describe the ground state of bulk iron. Thus, it is expected to be essential to use the GGA functional instead of the LSDA to correctly describe the magnetic ground state of an Fe monolayer.

B. Exchange interactions

To gain a better understanding of the FM-SS phase transition in the Fe(110) monolayer, we introduce an exchange interaction parameter within the effective Heisenberg Hamiltonian,

$$H_{\mathrm{eff}} = -\frac{1}{2}\sum_{i,j} J_{ij}\mathbf{e}_i \cdot \mathbf{e}_j, \qquad (1)$$

where J_{ij} denotes the exchange interaction parameter between the ith and jth neighbors and $\mathbf{e}_i$ is the unit vector representing

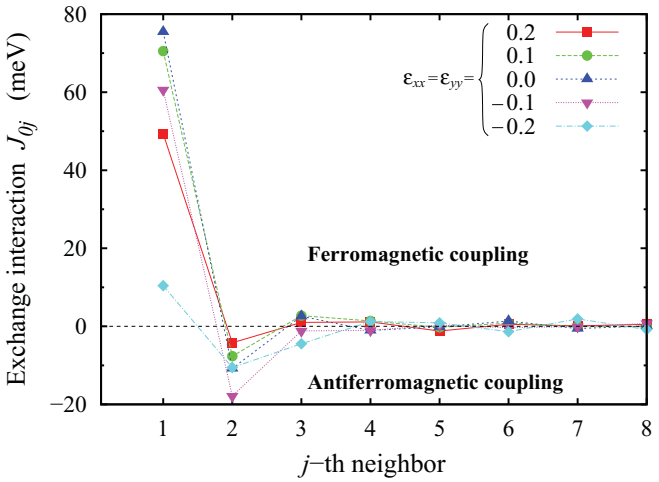

FIG. 4. (Color online) Exchange interaction parameter of the jth neighbor, J_{0j}, in the Fe(110) monolayer as a function of isotropic in-plane strain, $\varepsilon_{xx} = \varepsilon_{yy}$.

the direction of the local magnetic moment on the ith neighbor. Using Eq. (1), the total energy of the noncollinear SS state with $\mathbf{q}$, $E_{\mathrm{SS}}(\mathbf{q})$, is given by

$$E_{\mathrm{SS}}(\mathbf{q}) = -\frac{1}{2}\sum_{j} J_{0j}\exp(-i\mathbf{q}\cdot\mathbf{R}_{0j}), \tag{2}$$

where $\mathbf{R}_{0j}$ denotes the position vector of the jth neighbor with respect to the origin. In the classical frozen magnon approach, J_{0j} can be related to the SS wave excitation energy (magnon dispersion relation), $\Delta E(\mathbf{q}) = E_{\mathrm{SS}}(\mathbf{q}) - E_{\mathrm{FM}}$, by Fourier back-transformation,

$$J_{0j} = \frac{1}{N_{\mathbf{q}}}\sum_{\mathbf{q}} \Delta E(\mathbf{q})\exp(-i\mathbf{q}\cdot\mathbf{R}_{0j}), \tag{3}$$

where $N_{\mathbf{q}}$ denotes the number of $\mathbf{q}$ points in the Brillouin zone. We can thus evaluate the exchange parameter of the monolayer by summing the SS wave excitation energies for various $\mathbf{q}$ vectors using Eq. (3).

Figure 4 plots the exchange interaction parameter of the jth neighbor, J_{0j}, in the Fe(110) monolayer as a function of isotropic in-plane strain, $\varepsilon_{xx} = \varepsilon_{yy}$. Under strain-free conditions, $\varepsilon_{xx} = \varepsilon_{yy} = 0.0$, J_{01} has a large positive value of 75.5 meV. This indicates that the exchange interaction of the nearest neighbor tends to align the magnetic moment in the same direction as that of the origin (i.e., FM coupling). In contrast, J_{02} exhibits a relatively small negative value of −10.8 meV, indicating that the interaction from the second neighbor tends to reverse the magnetic moment direction (i.e., AFM coupling). J_{03} is positive (FM coupling), but its magnitude is one order of magnitude smaller than those of J_{01} and J_{02}, indicating that the exchange interaction from the third neighbors has a smaller influence than those from the first and second neighbors. Since J_{0j} ($j \geqslant 4$) is approximately zero, the fourth and farther neighbors do not exert a substantial influence. Therefore, the FM ground state can be stabilized by the competing exchange interaction between the larger ferromagnetically coupled nearest neighbors and the smaller antiferromagnetically coupled second neighbors. Under tensile strains, the positive J_{01} tends to decrease, whereas the negative J_{02} tends to increase. This suggests that both the FM and AFM couplings are weakened by the isotropic tension, which keeps the FM phase stable. In contrast, both J_{01} and J_{02} decrease rapidly under compression (i.e., compression weakens the FM interaction and strengthens the AFM interaction). This destroys the original balance and leads to the noncollinear SS ground state.

Figure 5 shows the exchange interaction parameters J_{01}, J_{02}, and J_{03}, as functions of in-plane anisotropic strains (ε_{xx}, ε_{yy}). Overall, the tension tends to increase J_{0j} and the compression tends to decrease J_{0j}. In particular, both the positive J_{01} and the negative J_{02} decrease rapidly around the strain region of $\varepsilon_{xx} = -0.1 \sim -0.2$ (as indicated by the relatively high density of contour lines). This indicates that the FM coupling from the first neighbors is weakened

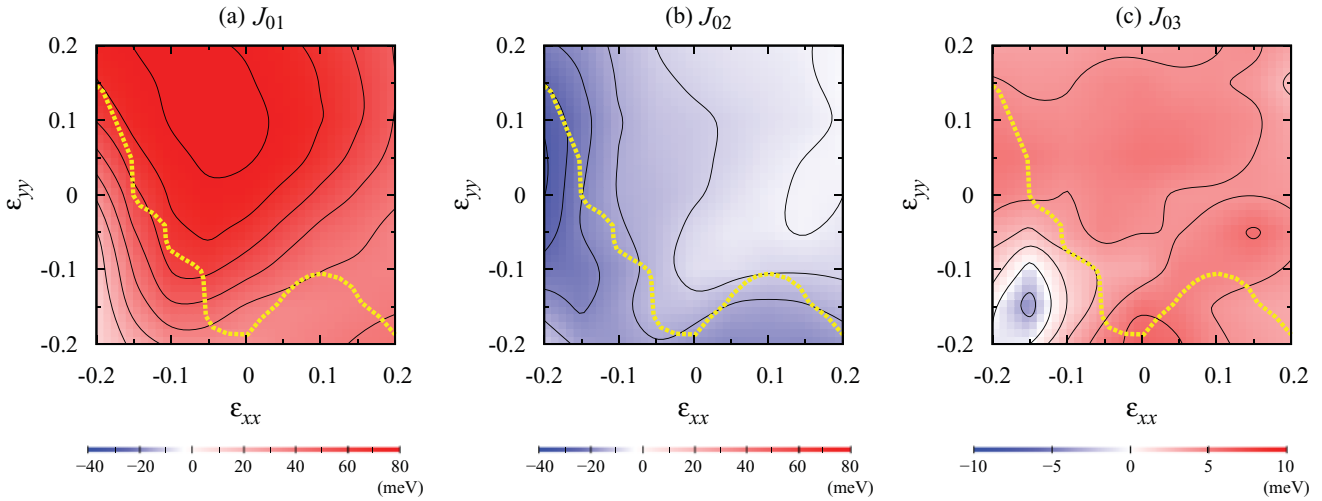

FIG. 5. (Color online) Exchange interaction parameters (a) J_{01}, (b) J_{02}, and (c) J_{03} as functions of in-plane strains (ε_{xx}, ε_{yy}). The yellow dashed lines indicate the FM-SS magnetic phase transition. Note that the contour of J_{03} is confined within the smaller range than those of J_{01} and J_{02}.

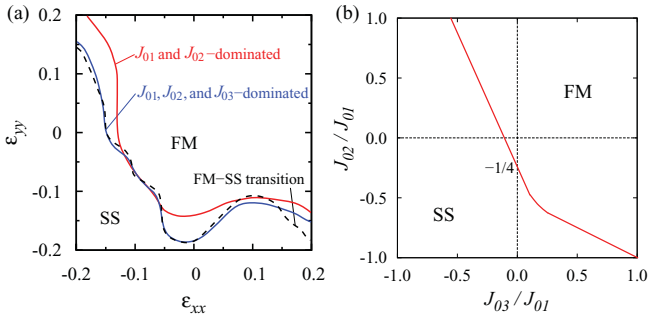

FIG. 6. (Color online) (a) FM-SS magnetic phase transition line calculated using the exchange parameters J_{01} and J_{02} (solid red line) and J_{01}, J_{02}, and J_{03} (solid blue line). For comparison, the black dashed line indicates the FM-SS transition directly obtained from *ab initio* total-energy calculations. (b) Magnetic phase diagram based on the Heisenberg model considering J_{01}, J_{02}, and J_{03}. The red line indicates the critical condition of the FM-SS phase transition.

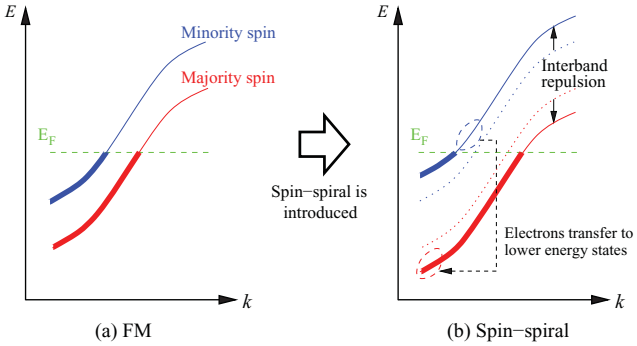

FIG. 7. (Color online) Schematic illustration of difference in the majority and minority spin band structures of the FM and SS states.

and that the AFM coupling for the second neighbors is strengthened remarkably by the compression along $[\bar{1}10]$ (in the x direction). This trend corresponds well to both the higher stability of the noncollinear SS state and the larger SS wave vector q_x observed under compressive ε_{xx}, as mentioned in the previous section [see also Figs. 3(a) and 3(b), respectively]. Note that, because J_{03} has a smaller magnitude than J_{01} and J_{02}, the contribution from the third neighbors is expected to be considerably smaller than those of the first and second neighbors.

Let us consider the critical condition for the FM-SS phase transition in terms of the exchange interaction parameters. The transition occurs when $E(\mathbf{q})$ in Eq. (2) becomes a minimum at $\mathbf{q} \neq \mathbf{0}$. Considering the exchange interaction features for which J_{01} and J_{02} are dominant, the critical condition for the FM-SS phase transition can be derived by applying $J_{01}, J_{02} \neq 0$, and $J_{0j} = 0$ $(j \geqslant 3)$ to Eq. (2). It is given by $J_{02}/J_{01} = -1/4$.[3] Figure 6(a) shows the FM-SS magnetic phase transition predicted by the critical condition based on only J_{01} and J_{02} (see the red line). For comparison, the black dashed line indicates the FM-SS transition directly obtained from *ab initio* total-energy calculations. The J_{01}-J_{02} dominated transition line coincides well with the actual FM-SS transition around the isotropic strain ($\varepsilon_{xx} = \varepsilon_{yy} = -0.1$). However, in the transition in the anisotropic strain region ($\varepsilon_{xx} \neq \varepsilon_{yy}$), they dissociate from each other. This discrepancy is expected to originate from the absence of J_{03}. We again consider the critical condition based on three exchange parameters, J_{01}, J_{02}, and J_{03}. The blue line in Fig. 6(a) indicates that the J_{01}-J_{02}-J_{03}-dominated transition line is in excellent agreement with the actual FM-SS transition for both isotropic and anisotropic strains. Here, the condition can be represented in the two-dimensional phase diagram as functions of J_{02}/J_{01} and J_{03}/J_{01}, as shown in Fig. 6(b).[50,51] This indicates that the FM-SS phase transition under the isotropic strain is dominated by the exchange interaction of the first and second neighbors, while the third neighbors additionally contribute to the transition under anisotropic strain.

C. Electronic band structures

Figure 7 shows a schematic illustration of the different majority and minority spin band structures of the FM and SS states. When the SS wave is introduced into the FM system, the majority and minority spin bands crossing the Fermi level E_F tend to separate from each other. The minority-spin band is pushed above the Fermi level and a portion of the band around E_F that was occupied in the FM phase becomes an unoccupied state (see the blue lines). On the other hand, the majority-spin band drops to a lower energy level (see the red lines). As a result of this interband repulsion due to the SS wave, electrons transfer from the higher minority-spin state to the lower majority-spin state, which reduces the total energy and thus stabilizes the noncollinear SS state. As discussed in Refs.[52–55], such stabilization of the SS structure can occur when both the majority and minority spin bands cross the Fermi level (which implies the formation of a Fermi surface). This is the electronic-level condition for noncollinear instabilities in FM systems.

To investigate the effect of SS waves on the electronic structures and the stabilization of SS structures under compression, we here analyze the electronic band structures of the Fe(110) monolayer for several SS wave vectors q_x. Figure 8 shows the electronic band structures of the Fe(110) monolayer with different SS wave vectors q_x under in-plane strains of $(\varepsilon_{xx}, \varepsilon_{yy}) = (0.0,0.0)$, $(-0.2, -0.2)$, $(-0.2, 0.0)$, and $(0.0, -0.2)$. For a strain-free monolayer [Fig. 8(a)], which exhibits the FM ground state, the electronic band structure at $q_x = 0$ corresponds to its two-dimensional geometry: The d_{xy}- and $d_{x^2-y^2}$-dominant bands are distributed over a wide energy range because they form direct and strong $dd\sigma$ bonds due to orbital alignment in the monolayer plane.[5] In contrast, the d_{yz}- and d_{zx}-dominant bands have a relatively narrow distribution because of the weaker interaction due to their orbital topologies being aligned out of the monolayer. The d_{z^2}-dominant band has the narrowest width because the corresponding orbitals are perpendicular to the monolayer. When we consider each pair of majority-spin and minority-spin bands, none of them satisfy the condition for the noncollinear SS structure, as discussed above. Thus, the system remains in the FM ground state.

On the other hand, at $\varepsilon_{xx} = \varepsilon_{yy} = -0.2$ four pairs of majority- and minority-spin bands of the d_{xy}, $d_{x^2-y^2}$, d_{yz}, and d_{z^2} orbitals fulfill the condition [see the thicker lines in Fig. 8(b); the red and blue lines indicate the majority and

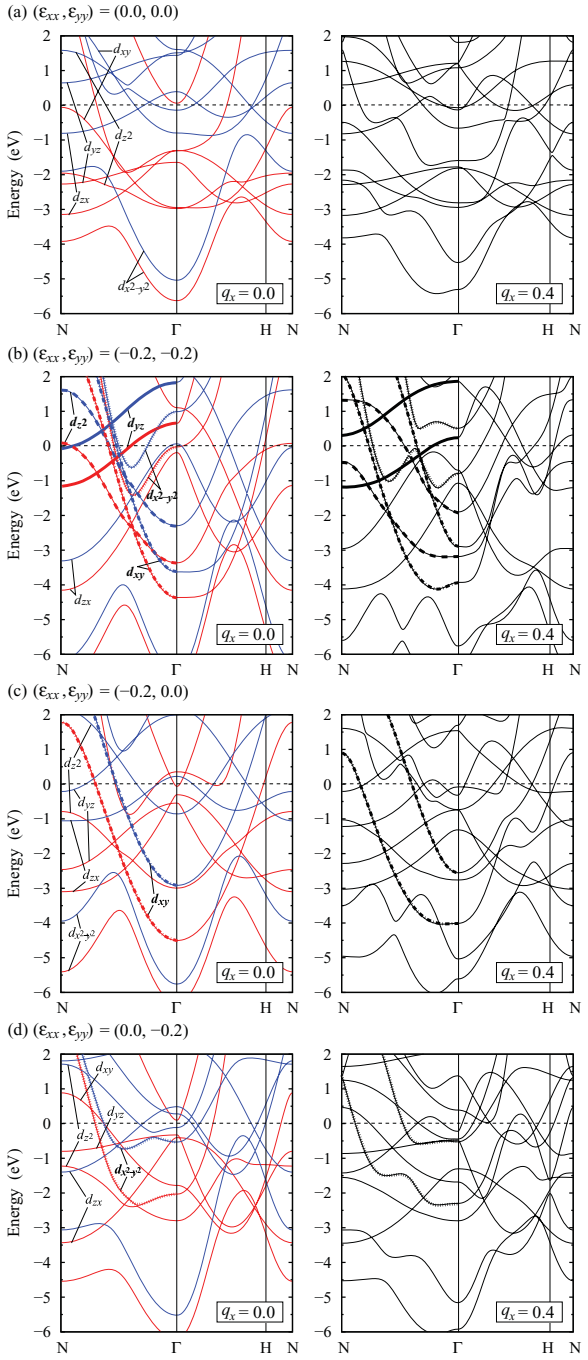

FIG. 8. (Color online) Electronic band structures of the Fe(110) monolayer with different SS wave vectors q_x under in-plane strains of (ε_{xx}, ε_{yy}) = (a) (0.0, 0.0), (b) (−0.2, −0.2), (c) (−0.2, 0.0), and (d) (0.0, −0.2). The red and blue lines, respectively, indicate majority-spin and minority-spin bands in the collinear FM state ($q_x = 0.0$).

minority spins, respectively]. These pairs of bands tend to disperse repulsively when an SS wave is introduced and the wave vector q_x increases. As explained above, these interband repulsions reduce the total energy of the system and stabilize the SS wave. In fact, the monolayer under this compressive strain exhibits the noncollinear SS state, as shown in the previous section. Note that the repulsion of bands is remarkable along the N-Γ line, which corresponds to the direction of

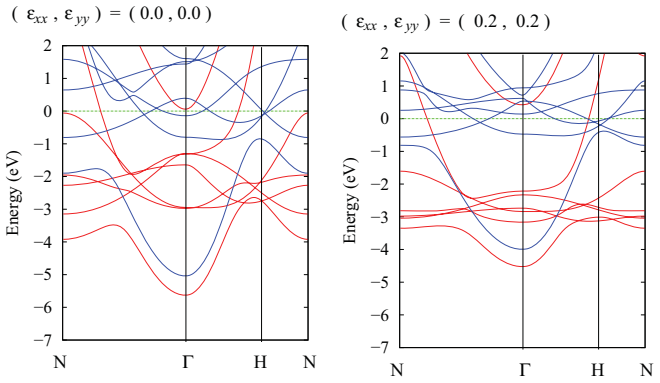

FIG. 9. (Color online) Electronic band structures of the ferromagnetic Fe(110) monolayer under the in-plane strains of (ε_{xx}, ε_{yy}) = (0.0,0.0) and (0.2, 0.2). The red and blue lines indicate the majority-spin and minority-spin bands, respectively.

the excited SS wave. In the same manner, under anisotropic strain conditions, (ε_{xx}, ε_{yy}) = (−0.2, 0.0) and (0.0, −0.2), the d_{xy}- and $d_{x^2-y^2}$-dominant bands, respectively, satisfy the condition, which also leads to the SS ground state. However, the monolayer under these anisotropic strains has fewer pairs of majority and minority spin bands that fulfill the requirement for the noncollinear SS state relative to the monolayer under isotropic strain. Recalling that the SS state is more stable for isotropic compression than anisotropic compression (see Fig. 3), the bands that satisfy the condition should directly contribute to the stability of the SS state.

Another important characteristic is that under compression, each band tends to be distributed over a wider energy range than the strain-free monolayer [e.g., compare Figs. 8(a) and 8(b)], and the applied tension reduces the bandwidth, as shown in Fig. 9. This is because the orbitals highly overlap each other due to a shortened bond length produced by compression. Clearly, as the bandwidth becomes broader, the number of the majority and minority spin bands that cross the Fermi level increases. This signifies that the compressive strain tends to stabilize the noncollinear SS state through the requirement for the SS state. On the other hand, applying a tensile strain narrows the bandwidth, which reduces the number of bands crossing the Fermi level. Therefore, the SS wave is excited and stabilized not by tension but by compression.

IV. CONCLUSION

We performed fully unconstrained first-principles spin-density-functional calculations to investigate the magnetic phase transition from collinear FM to noncollinear SS ordering in an Fe(110) monolayer under in-plane strain. The strain-free monolayer is in the FM ground state. The Fe(110) monolayer undergoes the FM-SS phase transition on the application of in-plane compression, while tension keeps the system FM. The stability and wavelength of the excited SS state are increased on applying further compressive strain, especially along [$\bar{1}$10]. Heisenberg-Hamiltonian–based analysis of the exchange interaction revealed that the FM-SS transition in an isotropically strained monolayer is dominated by competing exchange interactions between the ferromagnetically coupled first neighbor and the antiferromagnetically coupled second

neighbor, while the third neighbor also contributes to the transition under anisotropic strains. In addition, we demonstrated the stabilization mechanism of SS noncollinear magnetism from electronic band structures: The noncollinear SS state is stabilized in a monolayer under compression by the remarkable interband repulsion between the majority and minority spins.

ACKNOWLEDGMENTS

This work was supported in part by a Grant-in-Aid for Scientific Research (S) (Grant No. 21226005) and a Grant-in-Aid for Young Scientists (A) (Grant No. 23686023) from the Japan Society of the Promotion of Science (JSPS).

*shimada@cyber.kues.kyoto-u.ac.jp

[1] G. Autès, C. Barreteau, D. Spanjaard, and M. C. Desjonquères, J. Phys.: Condens. Matter **18**, 6785 (2006).

[2] M. Zelený, M. Sob, and J. Hafner, Phys. Rev. B **79**, 134421 (2009).

[3] M. Zelený, M. Sob, and J. Hafner, Phys. Rev. B **80**, 144414 (2009).

[4] T. Shimada, Y. Ishii, and T. Kitamura, Phys. Rev. B **81**, 134420 (2010).

[5] T. Shimada, J. Okuno, Y. Ishii, and T. Kitamura, J. Phys.: Condens. Matter **24**, 095303 (2012).

[6] T. Shimada, Y. Ishii, and T. Kitamura, Phys. Rev. B **84**, 174405 (2011).

[7] T. Shimada, Y. Ishii, and T. Kitamura, Phys. Rev. B **84**, 165452 (2011).

[8] G. A. Prinz, Science **282**, 1660 (1998).

[9] F. Li, R. M. Metzger, and W. D. Doyle, IEEE Trans. Magn. **33**, 3715 (1997).

[10] K. K. Lew and J. M. Redwing, J. Cryst. Growth **254**, 14 (2003).

[11] Y. C. Wang, I. C. Leu, and M. H. Hon, J. Cryst. Growth **237**, 564 (2002).

[12] H. J. Elmers, J. Hauschild, H. Höche, U. Gradmann, H. Bethge, D. Heuer, and U. Köhler, Phys. Rev. Lett. **73**, 898 (1994).

[13] M. Bode, O. Pietzsch, A. Kubetzka, S. Heinze, and R. Wiesendanger, Phys. Rev. Lett. **86**, 2142 (2001).

[14] A. Berger and H. P. Oepen, J. Magn. Magn. Mater. **121**, 102 (1993).

[15] M. Pratzer, H. J. Elmers, M. Bode, O. Pietzsch, A. Kubetzka, and R. Wiesendanger, Phys. Rev. Lett. **87**, 127201 (2001).

[16] M. Pratzer and H. J. Elmers, Phys. Rev. B **67**, 094416 (2003).

[17] K. Nakamura, Y. Takeda, T. Akiyama, T. Ito, and A. J. Freeman, Phys. Rev. Lett. **93**, 057202 (2004).

[18] Y. Takeda, K. Nakamura, T. Akiayama, and T. Ito, Appl. Surf. Sci. **244**, 485 (2005).

[19] K. Nakamura, T. Ito, and A. J. Freeman, J. Appl. Phys. **97**, 10A315 (2005).

[20] K. Nakamura, T. Akiyama, T. Ito, and A. J. Freeman, J. Appl. Phys. **105**, 07C304 (2009).

[21] A. J. Freeman and K. Nakamura, J. Magn. Magn. Mater. **321**, 894 (2009).

[22] K. Nakamura, N. Mizuno, T. Akiyama, T. Ito, and A. J. Freeman, J. Appl. Phys. **101**, 09G521 (2007).

[23] K. Nakamura, N. Mizuno, T. Akiyama, T. Ito, and A. J. Freeman, J. Appl. Phys. **99**, 08N501 (2006).

[24] N. Mizuno, K. Nakamura, T. Akiyama, and T. Ito, J. Phys.: Condens. Matter **19**, 365222 (2007).

[25] C. S. Wang, B. M. Klein, and H. Krakauer, Phys. Rev. Lett. **54**, 1852 (1985).

[26] D. J. Singh, W. E. Pickett, and H. Krakauer, Phys. Rev. B **43**, 11628 (1991).

[27] M. Zelený, D. Legut, and M. Sob, Phys. Rev. B **78**, 224105 (2008).

[28] H. C. Herper, E. Hoffmann, and P. Entel, Phys. Rev. B **60**, 3839 (1999).

[29] M. Friák, M. Sob, and V. Vitek, Phys. Rev. B **63**, 052405 (2001).

[30] L. Tsetseris, Phys. Rev. B **72**, 012411 (2005).

[31] M. Friák and M. Sob, Phys. Rev. B **77**, 174117 (2008).

[32] S. V. Okatov, A. R. Kuznetsov, Y. N. Gornostyrev, V. N. Urtsev, and M. I. Katsnelson, Phys. Rev. B **79**, 094111 (2009).

[33] P. Hohenberg and W. Kohn, Phys. Rev. **136**, B864 (1964).

[34] W. Kohn and L. Sham, Phys. Rev. **140**, A1133 (1965).

[35] C. Jo and J. I. Lee, Phys. Status Solidi B **241**, 1427 (2004).

[36] K. Nakamura, T. Ito, A. J. Freeman, L. Zhong, and J. F. de Castro, J. Appl. Phys. **93**, 6879 (2003).

[37] J. Schwitalla, B. L. Gyöfffy, and L. Szunyogh, Phys. Rev. B **63**, 104423 (2001).

[38] G. Kresse and J. Hafner, Phys. Rev. B **47**, 558 (1993).

[39] G. Kresse and J. Furthmüller, Phys. Rev. B **54**, 11169 (1996).

[40] P. E. Blöchl, Phys. Rev. B **50**, 17953 (1994).

[41] G. Kresse and D. Joubert, Phys. Rev. B **59**, 1758 (1999).

[42] G. Kresse, W. Bergermayer, and R. Podloucky, Phys. Rev. B **66**, 146401 (2002).

[43] J. P. Perdew, K. Burke, and M. Ernzerhof, Phys. Rev. Lett. **77**, 3865 (1996).

[44] E. G. Moroni, G. Kresse, J. Hafner, and J. Furthmüller, Phys. Rev. B **56**, 15629 (1997).

[45] D. Hobbs, G. Kresse, and J. Hafner, Phys. Rev. B **62**, 11556 (2000).

[46] L. M. Sandratskii, J. Phys.: Condens. Matter **3**, 8565 (1991).

[47] M. Marsman and J. Hafner, Phys. Rev. B **66**, 224409 (2002).

[48] J. A. Rayne and B. S. Chandrasekhar, Phys. Rev. **122**, 1714 (1961).

[49] H. J. Monkhorst and J. D. Pack, Phys. Rev. B **13**, 5188 (1976).

[50] S. Heinze, P. Kurz, D. Wortmann, G. Bihlmayer, and S. Blügel, Appl. Phys. A **75**, 25 (2002).

[51] S. Shallcross, A. E. Kissavos, S. Sharma, and V. Meded, Phys. Rev. B **73**, 104443 (2006).

[52] L. M. Sandratskii, J. Phys.: Condens. Matter **3**, 8587 (1991).

[53] M. Uhl, L. M. Sandratskii, and J. Kübler, J. Magn. Magn. Mater. **103**, 314 (1992).

[54] R. Lizárraga, L. Nordström, L. Bergqvist, A. Bergman, E. Sjöstedt, P. Mohn, and O. Eriksson, Phys. Rev. Lett. **93**, 107205 (2004).

[55] R. Lizárraga, L. Nordström, and O. Eriksson, Phys. Rev. B **75**, 024425 (2007).